文章编号：1001-9014(2021)02-0143-07

DOI：10. 11972/j. issn. 1001-9014. 2021. 02. 001

# Mechanism analysis of terahertz graphene electro-optic modulator with plasma structure

LI Jia-Bin*, WANG-Xiao-Hua, WANG Wen-Jie

(School of Electronics and Information, Xi'an Polytechnic University, Xi'an 710048, China)

**Abstract**: Based on the theory of plasmon resonance, we present a photon plasma ridge waveguide consisting of a metal/graphene/$Al_2O_3$/graphene stacking structure. The modulation performance is optimized through the design of the waveguide and plasma structures by analyzing the microscopic mechanism of photoelectric reaction. A low-insertion-loss near-infrared electro-optic modulator with a modulation rate of 730 GHz, energy consumption of 0. 7 fJ/bit, and 3-dB bandwidth of 3. 66 THz is achieved.

**Key words**: graphene-based electro-optic modulator, plasma structure, characteristic optimization, mechanism analysis

**PACS**: 41. 20. Jb, 42. 25. Bs, 42. 30. Lr, 42. 79. Gn

# 基于等离子体结构的太赫兹石墨烯电光调制器的机理分析

李佳斌*, 王晓华, 王文杰

(西安工程大学 电子信息学院,陕西 西安 710048)

**摘要**:基于等离子体共振机理,提出了一种包含金属/石墨烯/ $Al_2O_3$/石墨烯堆栈结构的等离子体脊型波导.基于光电效应的微观机理分析,通过设计波导结构和等离子体结构,优化调制器的性能.结果显示,电光调制器的插入损耗很低,工作在近红外波段,调制速率为730 GHz,能量损耗为0.7 fJ/bit,3-dB带宽为3.66 THz.

**关 键 词**:石墨烯电光调制器;等离子体结构;特性优化;机理分析

**中图分类号**:O439 **文献标识码**:A

## Introduction

Electro-optic modulator (EOM), as the core component of the optical fiber communication and integrated optics, has received wide attention recently. The demand for EOM with higher rate, smaller size, lower power consumption, and easy integration increases dramatically due to the rapid development of the optical fiber communication network and the application of optical interconnection on chip. At present, the material that is used to improve the performance of EOM is graphene, graphene-based EOM has the following advantages: graphene has a strong inter-band optical transition ability, which enhances the interaction between graphene and light, and the modulation performance will be improved; graphene-based EOM has higher modulation rates due to the fact that graphene has extremely high electron mobility [1-5]; graphene has wide operating wavelength bandwidth, and its operating frequency covers almost the entire optical communication working bandwidth, even to the mid-infrared, far-infrared, terahertz, and microwave range [6]; the photoconductivity of graphene is adjustable; the fabrication process is compatible with existing CMOS process technology[7-8].

In the past few years, researchers at home and abroad had conducted extensive research on graphene-based EOM, many research groups had reported excellent results [9-16]. In 2016, Zhang's team proposed an improved graphene-based light modulator structure with a 3dB modulation bandwidth of up to 35 GHz, showing good thermal stability [17]. In 2017, Lin *et al.* designed a graphene-based EOM that can achieve a modulation

**Received date**: 2020- 02- 09, **revised date**: 2020- 03- 03 **收稿日期**:2020- 02- 09,**修回日期**:2020- 03- 03

**Foundation items**: Supported by Research Project of Xi' an Polytechnic University (107020492) and National Natural Science Foundation of China (51905405)

**Biography**: LI Jia-Bin (1986- ), male, Jiamusi China, Ph. D. Research area involves photoelectric properties of two-dimensional materials and Ⅲ-Ⅴ compounds.

* **Corresponding author**: E-mail: 15991730364@163. com

depth of 8 dB/mm in the wavelength range of 2.05 m to 2.45 m [18]. In 2018, Liu et al. proposed a graphene/alumina multilayer stacked EOM based on photonic crystal nanobeams, with transmission and absorption modulation depths of 11.25 nm/eV and 12.50 nm/eV, respectively[19]. In 2018, Hu et al. designed a graphene-based polarization insensitive sensor modulator with insertion loss of less than 2 dB at the wavelength range of 35 nm (including c-band)[20].

In recent years, several research groups at home and abroad have carried out research on graphene-based plasma EOM. In 2017, Peng *et al.* proposed a novel graphene EOM based on the hybrid plasma effect, which can improve the modulation efficiency to 1.23 dB/m, introduce insertion loss of only 0.32 dB in the 3.6-m-long modulation region, and the modulation bandwidth is up to 480 GHz [21]. In 2019, Wang *et al.* designed a graphene/hexagonal boron nitride structure-based plasma EOM at the sub-wavelength scale, the results show that the modulation depth is up to 4 dB/μm, the transmission loss is 2.6 dB, the modulation speed is up to 39 GHz, and the energy loss is 21.2 fJ /bit [22].

However, monolayer graphene only has a light absorption rate of 2.3%, its optical response is weak. The interaction between light and matter in the graphene-based EOM is so weak that it is difficult to continuously improve the modulation efficiency and the reduce the device size. Surface plasmas have strong local property, which exhibit strong field restraint and field enhancement. By covering the surface of the graphene-based EOM with plasma structure, the interaction between the mode field and graphene can be enhanced [23-25], the modulation performance of EOM that can be operated in the terahertz, infrared, and visible light band is improved [26-28].

In this study, we investigate a graphene-based electro-optic modulator with plasma structure using the finite-element method implemented in the multi-physics software COMSOL. By designing the waveguide and plasma structure, the properties of EOM will be improved. The modulation mechanism of EOM by structure parameters will be analyzed through the microscopic mechanism of photoelectric reaction.

## 1 Device design and theoretical analysis

The structure of the electro-optic modulator is shown in Fig. 1(a), mainly composed of Si waveguide, graphene/$Al_2O_3$/graphene stacking structure, plasma structure, and $SiO_2$ substrate. The width and height of the waveguide are 400 nm and 200 nm, respectively. Two graphene layers are placed on top of the Si waveguide, which is isolated by $Al_2O_3$. The two graphene layers are extended from the opposite sides of the Si waveguide for metallization. A few nanometers of Ag, as the plasma structure, is placed on top of graphene layer. The thicknesses of the graphene and $Al_2O_3$ are 0.7 nm and 10 nm, respectively. The free-space wavelength is $\lambda$ = 1 550 nm. We assume that the electrodes are far away from the

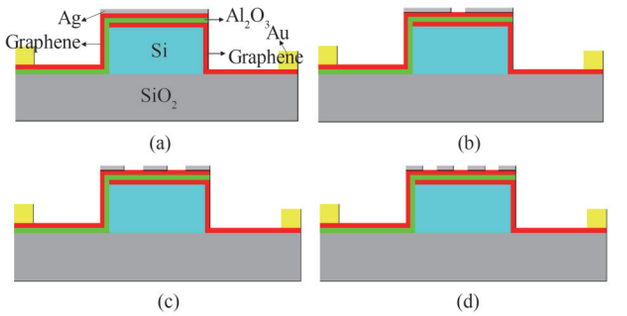


Fig. 1 Structures of the electro-optic modulator. The length of the modulator is 20 μm, the width and height of the substrate are 200 nm and 2 μm, respectively. The refractive index of $SiO_2$, Si, $Al_2O_3$ are 1.444, 3.42, and 1.595, respectively (a) single plasma structure, (b) double plasma structures, (c) three plasma structures, (d) four plasma structures

图1 电光调制器的结构。调制器的长度为20 μm,衬底的宽度和高度分别为200 nm、2 μm。$SiO_2$、Si、$Al_2O_3$的折射率分别为1.444、3.42、1.595 (a)单一等离子体,(b)双等离子体,(c)三个等离子体,(d)四个等离子体

Si waveguide, so that they do not influence the optical mode.

According to the dispersion relation of surface plasma waves, surface plasma waves can be excited only when the wave vector of the surface plasma is larger than the light wave vector in the medium and the tangential wave vector satisfies the matching condition. The wave vector of the surface plasma wave in the x direction can be expressed as:

$$k_x = k_0 \sqrt{\frac{\varepsilon_m \varepsilon_d}{\varepsilon_m + \varepsilon_d}} \quad , \quad (1)$$

where $\varepsilon_m$ is the real part of the dielectric constant of metallic plasma structure, $\varepsilon_d$ is the dielectric constant of the medium.

For the metallic plasma structure and medium, $\varepsilon_m$ and $\varepsilon_d$ are greater than 1, $\varepsilon_m$ is greater than $\varepsilon_d$. The wave vector of the surface plasma wave in the x direction can be expressed as:

$$k_x = k_0 \sqrt{\frac{\varepsilon_m \varepsilon_d}{\varepsilon_m + \varepsilon_d}} > k_0 \quad . \quad (2)$$

When light is emitted from the medium into the interface between the plasma structure and the medium, the wave vector in the $x$ direction can be expressed as:

$$\tilde{k}_x = k_0 n_x \sin\theta > k_0 \quad . \quad (3)$$

From Eqs. 2-3 we can see that the matching principle of wave vector can be satisfied under certain conditions, the wave vectors can be coupled, and the surface plasma waves can be excited.

To quantify the mode field characteristics and enhancement of the equidistant waveguide, the normalized mode field area is defined as [35-37]:

$$\frac{A_{\text{eff}}}{A_0}(\mu = 0\ \text{eV}) \quad , \quad (4)$$

$$A_0 = \frac{\lambda^2}{4} \quad , \quad (5)$$

$$A_{\text{eff}} = \iint \frac{W(r)\,\mathrm{d}^2 r}{\max\left(W(r)\right)} \quad , \quad (6)$$

$$W(r,\omega) = \frac{1}{2}\mathrm{Re}\left\{\frac{\mathrm{d}\left(\omega\varepsilon(r,\omega)\right)}{\mathrm{d}\omega}\right\}\left|E(r,\omega)\right|^2 + \frac{1}{2}\mu_0\left|H(r,\omega)\right|^2 \quad , \quad (7)$$

where $A_0$ is the area of the diffraction limit in free space, $A_{\text{eff}}$ is the ratio of the total energy to the maximum energy density, $W(r)$ is electromagnetic field density, $E(r)$ is the electric field density, $H(r)$ is the magnetic density.

The smaller the normalized mode field area of the modulator, the greater the energy density of the electromagnetic field can be, facilitating the light-graphene interaction.

Based on the device structure, the modulation speed ($f$) of the modulator can be expressed as:

$$f = \frac{1}{2\pi RC} \quad , \quad (8)$$

where $R$ and $C$ represent the resistance and capacitance of the modulator, respectively. $R$ is composed of $R_c$ (the resistance between the metal and graphene layer) and $R_g$ (the resistance of the graphene sheet), while $C$ is composed of the quantum capacitance in each graphene sheet $C_Q$ and oxide plate capacitance $C_p$ connected in series.

The quantum capacitance per unit area $C_Q$ can be expressed as [32]:

$$C_Q = \frac{2e^2 kT}{\pi\left(\hbar v_F\right)^2}\ln\left[2\left(1+\cosh\frac{E_F}{kT}\right)\right] \quad , \quad (9)$$

where $e$ is the electron charge, $k$ is the Boltzmann constant, $T$ is the temperature, $\hbar$ is the reduced Planck constant, $v_F$ is the Fermi velocity, and $E_F$ is the Fermi level.

By utilizing the simple parallel plate capacitor model, $C_p$ can be calculated as:

$$C_p = \frac{\varepsilon_0\varepsilon_x}{\mathrm{EOT}} \quad , \quad (10)$$

where $\varepsilon_0$ is the dielectric constant of vacuum, $\varepsilon_x$ is the relative permittivity of the medium, and ETO is the equivalent thickness of $Al_2O_3$ between the two-layer graphene.

The graphene sheet resistance $R_g$ can be calculated as:

$$R_g = \frac{L_g}{\sigma w_g d} \quad , \quad (11)$$

where $\sigma$ is the conductivity of graphene, $d$ is the thickness of graphene, $W_g$ is the width of graphene, and $L_g$ is the length of graphene.

The contact resistance between the metal and graphene $R_c$ can be expressed by the Landauer formula as [33]:

$$R_c = \frac{h}{4e^2}\cdot\frac{1}{TM} \quad , \quad (12)$$

where $M$ is the number of conduction modes in graphene and $T$ is the carrier transmission probability. The number of quantum modes $M$ can be expressed as:

$$M = \frac{\Delta E_F W_g}{\pi\hbar v_F L_g} \quad , \quad (13)$$

where $\Delta E_F$ is the gap between the Fermi level and Dirac energy.

The energy consumption $E$ can be expressed as:

$$E = \frac{1}{4}CV_{pp}^2 \quad , \quad (14)$$

where $V_{pp}$ is the peak - to - peak voltage.

## 2　Results and discussion

The performance of modulator can be enhanced due to the interaction between graphene and light, the optical properties of graphene affect the performance of modulator to a large extent. In the graphene-based modulator, even a small variation in the refractive index of graphene may lead to a large shift of the resonant wavelength, the switching "on/off" of the modulator depends on the optical refractive index of graphene. The inter-band transition of graphene can be controlled by tuning the Fermi level ($E_F$) by electrical gating, optical excitation, or chemical doping [29-31], which has a large influence on its refractive index. Here, the refractive index of graphene is modulated by adding a voltage on graphene. The refractive index of graphene as a function of the voltage that is shown in Ref. 34 is cited in our research. The graphene exhibits the maximum real part of the refractive index at approximately 4 V, the refractive index transforms from dielectric to metal at approximately 6 V. In this study, voltages of 2.8 V, 4.2 V, 5.4 V, and 6.6 V corresponding to the refractive indices of graphene of 2.5, 4.5, 1.33, and 0.17 respectively are selected to tune the properties of EOM. The voltage of 6.6 V is considered to be the "OFF" state point.

The metal plasma structure in nanoscale has a unique capability to concentrate light at the deep-subwavelength scale. The strong in-plane electric field confinement of the plasmonic mode brings a high in-plane electric field density at the edges of plasmonic structure and thus enhances interaction with graphene. The surface plasmon polaritons can be excited effectively at the interface between metal and medium only if the plasma wave at the interface satisfies the matching conditions that are shown in Eqs. 2-3, one of the mainly structure factors to match these conditions is the height of the metal plasma structure. Figure 2(a) shows the transmission spectra of modulator for different heights of the metal plasma structure. Modulation depths that are larger than 35 dB are observed in all the curves. The modulation depths corresponding to different heights of metal plasma structure differ slightly between each other, except for the case with 5 nm height of metal plasma structure; the resonant wavelength exhibits a red-shift trend with respect to the height of the metal plasma structure. Figure 2(b) shows the calculated 3-dB bandwidth of modulator for different heights of the metal plasma structure. It is seen that the metal plasma structure of 5 nm height corresponds to the minimum 3-dB bandwidth, the metal plasma structure of 3 nm height corresponds to the maximum

3-dB bandwidth. As the height of the metal plasma structure increases, the curve of 3-dB bandwidth presents a non-monotonic trend. This is because that the decrease of thickness of the metal plasma structure will squeeze the localized plasmon to be near the location of the graphene, and apparently the strong field localization will enhance the light-graphene interaction, the 3-dB bandwidth of modulator increases gradually with the decrease of thickness of the metal plasma structure. When the thickness of the metal plasma structure is less than 3 nm, the conditions for plasmon excitation cannot be completely satisfied, the 3dB-bandwidth gradually decreases with the further reduction of the thickness of the metal plasma structure. By balancing the modulation depth and 3-dB bandwidth, the height of the plasma structure is set to 3 nm.

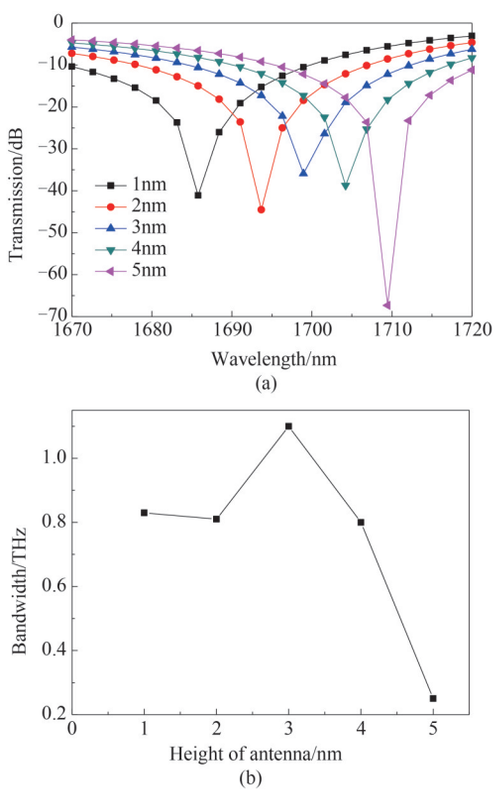


Fig. 2 Modulation performances of modulator for different heights of plasma structure (a) transmission spectra, (b) 3-dB bandwidth
图2 不同等离子体结构的高度对调制器调制性能的影响(a)传输谱,(b) 3-dB带宽。

It is known that only the electric field components parallel to graphene contribute to the light absorption property of graphene. This selectivity requests special structure that can strongly confine in-plane electric field components in graphene. Since the plasma structure can enhance in-plane electric field density at the interface between graphene and plasma structure, the performance of the modulator will be improved. This means that how to further enhance the electric field is a key problem. Based on the structure of the electro-optic modulator in

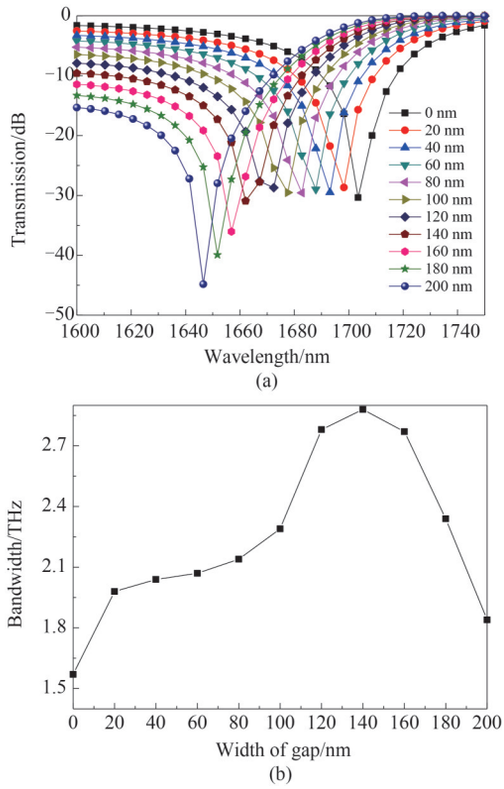


Fig. 3 Modulation performances of modulator for different gap widths between the two plasma structures (a) Transmission spectra, (b) 3-dB bandwidth
图3 两个等离子体结构之间间隙宽度的变化对调制器调制性能的影响(a)传输谱,(b) 3-dB带宽

Fig. 1(a), the metal plasma structure is divided into two part as shown in Fig. 1(b). The gap between two plasma structures is tens or hundreds of nanometers wide, which is much smaller than the wavelength. This kind of modulator structure supports higher in-plane electric field Bloch mode due to the fact that the electric field is highly confined in the gap laterally, the interference of a narrow resonance with a broad continuum of states leads to the enhancement of optical transmission. By calculating the Eqs. 4-7 we find that the normalized mode field area of the double-plasma based modulator is smaller than that of single-plasma based modulator, implying strong interaction between light and graphene. Figure 3(a) shows the transmission spectra of modulator for different widths of gap between the two plasma structures. Modulation depths that are larger than 30 dB are observed in all the curves. The modulation depths corresponding to different widths of gap differ slightly between each other as the width of gap is smaller than 160 nm. The resonant wavelength exhibits a blue-shift trend with respect to the width of gap between the two plasma structures. Figure 3(b) shows that the calculated 3-dB bandwidth increases first and then decreases with the increase of gap width, the gap width of 140 nm corresponds to the maximum 3-dB bandwidth. The results above imply that the plasmon resonances in the horizontal direction are excited by a horizontal electric field in the presence of the gap between the two plasma structures, which enhanced the light -

matter interaction and improved the transmission performance of the modulator. The horizontal electric fields from plasmon resonance of the two plasma structures are superimposed and enhanced by interference, gradually increasing in-plane electric field density. The condition for the interference enhancement of electric field is no longer fully satisfied when the width of gap of the two plasma structures is greater than 140 nm, the 3-dB bandwidth decreases as the gap width increases. By balancing the modulation depth and 3-dB bandwidth, the width of gap of the two plasma structures is set to 140 nm.

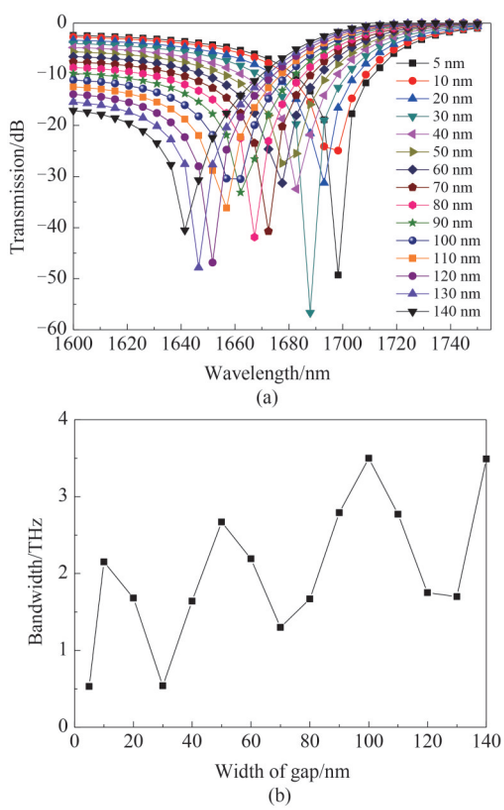


Fig. 4　Modulation performances of modulator for different gap widths between adjacent plasma structures. The plasma structure is divided into three equal parts and the two gaps are of equal width (a) transmission spectra, (b) 3-dB bandwidth
图4　相邻等离子体结构之间间隙宽度的变化对调制器调制性能的影响。等离子体结构被两个宽度相等的间隙平均分割为三个部分(a) 传输谱,(b) 3-dB带宽

Further, we investigate the electro-optic modulators with three and four plasma structures as shown in Figs. 1 (c-d). Figure 4 (a) shows the transmission spectra of three-plasma based modulator for different widths of gap between the two plasma structures. It is seen that the modulation depths that are larger than 25 dB are observed in all the curves, the modulation depths corresponding to different gap widths varies greatly. The resonant wavelength exhibits a blue-shift trend with respect to the width of gap between the two plasma structures. Figure 4 (b) shows the calculated 3-dB bandwidth of three-plasma based modulator for different widths of gap between the two plasma structures. The 3-dB bandwidth exhibits disordered variations. This demonstrates that the light-matter interaction could be enhanced in some cases by the segmented horizontal electric field or weakened in other cases. We can infer that the condition for the interference enhancement of electric field is satisfied when the width of gap between the two plasma structures is set to some values, but not when the gap width is set to other values. The gap width of 100 nm between the two plasma structures (the width of plasma structure is 66.67 nm) in the three-plasma based modulator corresponds to the maximum 3-dB bandwidth of 3.5 THz, which is larger than that in the double-plasma based modulator.

Figure 5 shows the transmission spectra and the calculated 3-dB bandwidth of four-plasma based modulator for different widths of gap between the two plasma structures, transmission behavior and the trend of 3-dB bandwidth curve that are like that of three-plasma based modulator that is shown in Fig. 4 are observed. A maximum 3-dB bandwidth (corresponding to a gap width of 75 nm or plasma structure width of 43.75 nm) of 3.66 THz is observed, which is larger than that in the three-plasma based modulator. The results above demonstrate that the in-plane electric field parallel to graphene can be enhanced by adjusting the width of gap between the two plasma structures due to the degree to which the condition for the interference enhancement of electric field is satisfied, thus the performance of the modulator is improved. It is foreseen that the 3-dB bandwidth will increase further by adjusting the amount of plasma structure and the width of gap between the two plasma structures.

We consider the single- and double-plasma based modulators as examples, whose transmissions as a function of the wavelength under different voltages are shown in Fig. 6. For the single-plasma based modulator, the resonant wavelength is almost unchanged, approximately 1 705.6 nm. Based on this resonant wavelength, the transmission of light at the "OFF" state (voltages of 6.6 V corresponding to refractive indices of graphene of 0.17) is approximately 20 dB. For the double-plasma based modulator, the resonant peak exhibits a significant blue-shift trend owing to the increase in the refractive index of graphene. Wide band between the resonant wavelength at the "on" state and the resonant wavelength at the "OFF" state is observed, the modulation range of the modulator has been expanded greatly. The transmission of light at the "OFF" state is smaller than 10 dB based on the different resonant wavelengths. The weak transmission of light at the "OFF" state corresponding to the resonant wavelength represents the excellent performance of modulator in some ways due to the small transmission loss of light. Figure 7 shows that the changes of 3-dB bandwidth of modulator with the refractive index of graphene, the maximum 3-dB bandwidths are observed at a bias voltage of 4.2 V (corresponding to the maximum refractive index of graphene) in single- and double-plasma based modulators. Furthermore, the 3-dB bandwidths of the double-plasma based modulator are bigger than that of single-plasma based modulator structure in different bi-

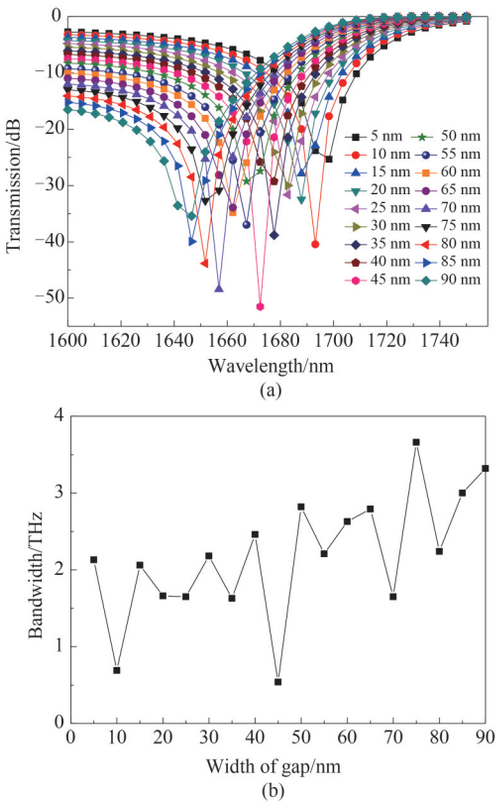


Fig. 5 Modulation performances of modulator for different gap widths between adjacent plasma structures. The plasma structure is divided into four equal parts and the three gaps are of equal width (a) transmission spectra,; (b) 3-dB bandwidth

图5 相邻等离子体结构之间间隙宽度的变化对调制器调制性能的影响。等离子体结构被三个宽度相等的间隙平均分割为四个部分。(a) 传输谱,(b) 3-dB带宽

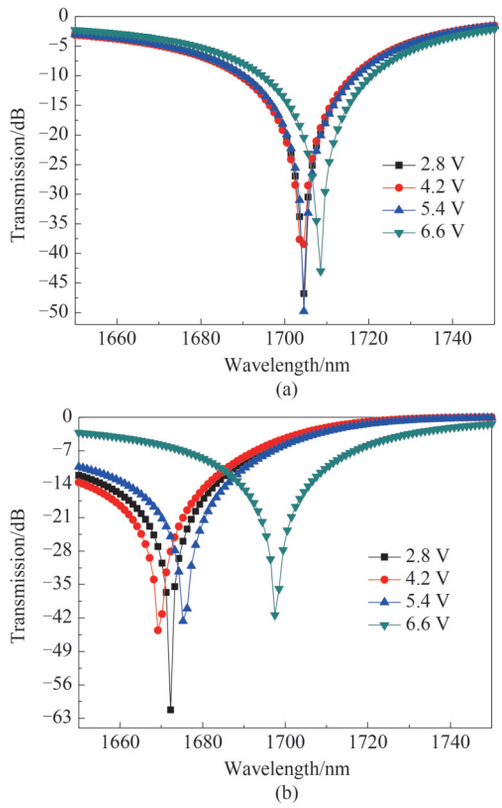


Fig.6 Transmission spectra as a function of the wavelength corresponding to different bias voltages (a) single-plasma based modulator structure, (b) double- plasma based modulator structure

图6 不同偏置电压下传输谱随波长的变化(a) 基于单等离子体结构的调制器,(b) 基于双等离子体结构的调制器

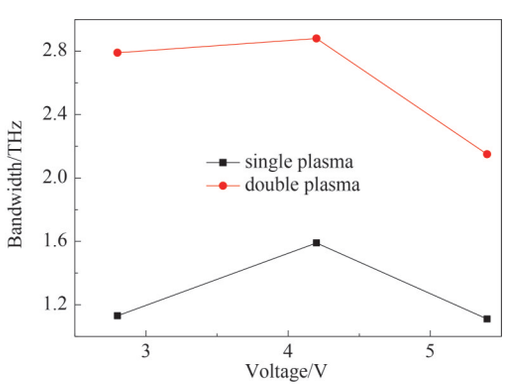


Fig. 7 3-dB bandwidths of single- and double-plasma modulators under different bias voltages

图7 不同偏置电压下单等离子体结构和双等离子体结构调制器的3-dB带宽

as voltage due to the degree of interference enhancement of the electric field paralleled to graphene.

According to the Eqs. 8-14, the equivalent resistance $R$, equivalent capacitance $C$, modulation speed $f$, and the energy consumption $E$ are calculated, as shown in Table 1 (all calculations are based on the optimal structure and parameters discussed above). Based on the Eq. 10, The calculation of capacitance includes the effect of carrier transport characteristics of heterojunction interface on the dielectric constant. Considering various scattering mechanisms in carrier transport, the calculation result of traditional drift-diffusion model has a relatively big error. In this paper, Monte Carlo method is used to characterize dielectric materials with non-mutational refractive index function, so as to optimize the calculation of equivalent capacitance.

From Table 1 we can see that strong correlation between the modulation speed and voltage is observed, the modulation speed increases with the voltage; the maximum modulation speed is calculated to be 730 GHz under the bias voltage of 5.4 V. The energy consumption $E$ significantly varies with the voltage; the smallest energy consumption is calculated to be 0.7 fJ/bit under the bias voltage of 5.4 V, corresponding to the smallest difference from the "OFF"-state voltage. Figure 8 shows that slightly different 3-dB bandwidths are observed at bias voltages of 4.2 V and 5.4 V. By balancing the energy consumption and 3-dB bandwidth, we reveal that the bias voltage of 5.4 V is appropriate.

## 3 Conclusion

Based on the concept of localized plasmon resonance, we presented the photon plasma ridge waveguide consisting of the metal/graphene/$Al_2O_3$/graphene stacking

**Table 1 Modulation speeds and energy consumptions of the modulator under different bias voltages**
**表1 不同偏置电压下调制器的调制速度和能量损耗**

| Bias voltage /V | $R$ /Ω | $C$/fF | $f$ /GHz | $E$ /(fJ/bit) |
|---|---|---|---|---|
| 2.8 | 155 | 1.943 | 527 | 7.01 |
| 4.2 | 127 | 1.949 | 645 | 2.81 |
| 5.4 | 112 | 1.952 | 730 | 0.70 |

structure. The plasma structure that can improve the modulation performance of modulator was designed and the light - matter interaction was enhanced owing to the plasmon resonances in the horizontal direction that is excited by the horizontal electric field. The optimization of the gap between adjacent plasmon structures showed that a larger 3-dB bandwidth could be achieved by increasing the number of plasmon structures. Furthermore, multi-plasma structures effectively reduced the transmission loss. According to the simulation results using the multi-physics software COMSOL, a terahertz near-infrared EOM with a modulation rate of 730 GHZ and energy consumption of 0.7 fJ/bit was achieved. The demonstrated excellent performances satisfy the application requirements of modern photonic integrated circuits.

## References


[1] Mayorov A S, Gorbachev R V, Morozov S V, *et al*. Micrometer-scale ballistic transport in encapsulated graphene at room temperature [J]. *Nano Lett*. 2011, **11**: 2396.
[2] Bolotin K I, Sikes K J, Jiang Z, *et al*. Ultrahigh electron mobility in suspended graphene [J]. *Solid State Commun*. 2008, **146** (9): 351-355.
[3] Gan X, Shiue R J, Gao Y, *et al*. Chip-integrated ultrafast graphene photodetector with high responsivity [J]. *Nat. Photonics*, 2013, **7** (11): 883-887.
[4] Hong X, Posadas A, Zou K, *et al*. High-mobility few-layer graphene field effect transistors fabricated on epitaxial ferroelectric gate oxides[J]. *Phys. Rev. Lett*. 2009, **102**(13): 136808.
[5] S. Winnerl, M. Orlita, P. Plochocka, *et al*. Carrier relaxation in epitaxial graphene photoexcited near the Dirac point[J]. *Phys. Rev. Lett*. 2011, **107**(23): 237401.
[6] R. R. Nair, P. Blake, A. N. Grigorenko, *et al*. Fine structure constant defines visual transparency of graphene[J]. *Science*, 2008, **320** (5881): 1308-1308.
[7] K. S. Kim, Y. Zhao, H. Jang, *et al*. Large-scale pattern growth of graphene films for stretchable transparent electrodes [J]. *Nature*, 2009, **457**(7230): 706-710.
[8] S. Bae, H. Kim, Y. Lee, *et al*. Roll-to-roll production of 30-inch graphene films for transparent electrodes [J]. *Nat. Nanotechnol*. 2010, **5**(8): 574-578.
[9] V. J. Sorger, R. Amin, J. B. Khurgin, *et al*. Scaling vectors of atto-Joule per bit modulators[J] *J. Opt*. 2018, **20**(1): 014012.
[10] A. N. Tait, T. F. Lima, E. Zhou, *et al*. Neuromorphic photonic networks using silicon photonic weight banks [J]. *Sci. Rep*. 2017, **7**: 7430.
[11] K. Liu, S. Sun, A. Majumdar, *et al*. Fundamental Scaling Laws in Nanophotonics[J]. *Sci. Rep*. 2016, **6**: 37419.
[12] M. Liu, X. Yin, E. Ulinavila, *et al*. A graphene-based broadband optical modulator[J]. *Nature*, 2011, **474**(7349): 64-67.
[13] M. Liu, X. Yin, X. Zhang. Double-layer graphene optical modulator [J]. *Nano Lett*. 2012, **12**(3): 1482-1485.
[14] S. J. Koester, M. Li. High-speed waveguide-coupled graphene-on-graphene optical modulators [J]. *Appl. Phys. Lett*. 2012, **100** (17): 611.
[15] K. Kim, J. Y. Choi, T. Kim, *et al*. A role for graphene in silicon-based semiconductor devices[J]. *Nature*, 2011, **479**(7373): 338-344.
[16] Y. T. Hu, M. Pantouvaki, S. Brems, *et al*. Broadband 10 Gb/s graphene electro-absorption modulator on silicon for chip-level optical interconnects[C]. IEEE International Electron Devices Meeting, San Francisco, 2014, 5.6.1-5.6.4
[17] Dalir H, Xia Y, Wang Y, *et al*. Athermal broadband graphene optical modulator with 35 GHz speed[J]. *Acs Photonics*, 2016, **3**(9): 1564-1568.
[18] Lin H T, Song Y, Huang Y Z, *et al*. Chalcogenide glass-on-graphene photonics[C]. CLEO: Science and Innovations, California, 2017, STh4I.5.
[19] Liu H Q, Liu P G, Bian L A, *et al*. Electro-optic modulator side-coupled with a photonic crystal nanobeam loaded graphene/$Al_2O_3$ multilayer stack[J]. *Opt. Express*, 2018, **8**(4): 761-774.
[20] Hu X, Wang J. Design of graphene-based polarizationinsensitive optical modulator[J]. *Nanophotonics*, 2018, **7**(3): 651-658.
[21] Peng X L, Hao R, Ye Z, *et al*. Highly efficient graphene-on-gap modulator by employing the hybrid plasmonic effect [J]. *Opt. Lett*. 2017, **42**(9): 1736-1739.
[22] Wang B B, Blaize S, Seok J B, *et al*. Plasmonic-based subwavelength graphene-on-hBN modulator on silicon photonics[J]. *IEEE J. Sel. Top. Quantum Electron*. 2019, **25**(3): 4600706.
[23] Peng X L, Hao R, Ye Z, *et al*. Highly efficient graphene-on-gap modulator by employing the hybrid plasmonic effect [J]. *Opt. Lett*. 2017, **42**(9): 1736-1739.
[24] Huang B, Lu W, Liu Z, *et al*. Low-energy high-speed plasmonic enhanced modulator using graphene[J]. *Opt. Express*, 2018, **26**(6): 7358-7367.
[25] Wang B B, Blaize S, Seok J B, *et al*. Plasmonic-based subwavelength graphene-on-hBN modulator on silicon photonics[J]. *IEEE J. Sel. Top. Quantum Electron*, 2019, **25**(3): 4600706.
[26] Yao Y, Kats M A, Geneve Pt, *et al*. Broad electrical tuning of graphene-loaded plasmonic antennas[J].*Nano Lett*.2014,**13**(3): 1257-1264.
[27] Kim J, Son H, Cho D J, *et al*. Electrical control of optical plasmon resonance with graphene [J]. *Nano Lett*. 2012, **12**(11): 5598 - 5602.
[28] Majumdar A, Kim J, Vuckovic J, *et al*. Electrical control of silicon photonic crystal cavity by graphene [J]. *Nano Lett*. 2013, **13**(2): 515-518.
[29] Wang F, Zhang Y B, Tian C S, *et al*. Gate-variable optical transitions in graphene[J]. *Science*, 2008, **320**: 206-209.
[30] Maiti R, Haldar S, Majumdar D, *et al*. Hybrid opto-chemical doping in Ag nanoparticle-decorated monolayer graphene grown by chemical vapor deposition probed by Raman spectroscopy[J]. *Nanotechnology*, 2017, **28**: 075707.
[31] Lee J, Novoselov K S, Shin H S. Interaction between metal and graphene: dependence on the layer number of graphene[J]. *ACS Nano*. 2011, **5**: 608-612.
[32] Scher S, Roulleau P, Molito F, *et al*. Quantum capacitance and density of states of graphene[J]. *Appl. Phys. Lett*. 2010, **96**(15):152104.
[33] Xia F, Perebeinos V, Lin Y M, *et al*. The origins and limits of metal-graphene junction resistance [J]. *Nat. Nanotechnol*, 2011, **6**: 179-184.
[34] Wu L, Liu H X, Li J B, *et al*. A 130 GHz electro-optic ring modulator with double-layer graphene[J]. *Crystals*, 2017, **7**: 65.
[35] Zhang Z, Wang J. Long-range hybrid wedge plasmonic waveguide [J]. *Scientific Reports*, 2014, **4**: 6870.
[36] Gui C, Wang J. Wedge hybrid plasmonic THz waveguide with long propagation length and ultra-small deep-subwavelength mode area [J]. *Scientific Reports*, 2015, **5**: 11457.
[37] Zheng K, Zheng X, Dai Q, *et al*. Hybrid rid-slot-rid plasmonic waveguide with deep-subwavelength mode confinement and long propagation length [J]. *AIP Adv*. 2016, **6**(8): 824-830.